❏ 5185

# Phase structures-based hybrid approaches for defect detection in vials

**Vishwanatha C. R.[1,2], Asha V.[1]**

[1]Research Centre-Department of Master of Computer Applications, New Horizon College of Engineering, Bengaluru, Affiliated to Visvesvaraya Technological University, Belagavi, Karnataka, India
[2]Department of Master of Computer Applications, Nitte Meenakshi Institute of Technology, Yelahanka, Bengaluru, Karnataka, India

## Article Info

## ABSTRACT

Quality control and assurance in pharmaceutical vial manufacturing are paramount to ensure drug safety and efficacy. Defects such as cracks, bubbles, black spots, and wrinkles can compromise product quality and patient safety. This study proposes a novel methodology that integrates fast non-local means (FNLM) filtering with hybrid image processing techniques to detect these defects. Previous approaches have often struggled with subtle anomalies in texture and surface features. The proposed solution leverages phase structure analysis, utilizing phase stretch transform (PST) to effectively highlight subtle anomalies by extracting features sensitive to phase variations. These features are further refined using Gaussian filtering, with Otsu thresholding applied for precise segmentation and defect boundary identification. Morphological dilation enhances detection speed and accuracy, while region of interest (ROI) identification aids in localizing defects and facilitating decision-making. The system demonstrates significant improvements in quality control, achieving high performance metrics: precision (98.85%), recall (98.57%), accuracy (98.36%), specificity (98.0%), and F1-score (98.71%). It also achieves impressive AUC-ROC (98.18%) and AUC-PR (99.08%) values, demonstrating its robustness and suitability for defect detection in pharmaceutical vials.

*Corresponding Author:*

Vishwanatha C. R.
Research Centre-Department of Master of Computer Applications, New Horizon College of Engineering,
Bengaluru, Affiliated to Visvesvaraya Technological University
Belagavi-590018, Karnataka, India
Email: vishwanathcr@gmail.com; vishwanatha.cr@nmit.ac.in

## 1. INTRODUCTION

Various types of containers are commonly used for pharmaceutical drug packaging such as syringes, vials, ampoules, and cartridges. Vials have gained universal acceptance due to their inertness, stability, and defiance of chemical reactions. Authorities of pharmacopeia have defined the standards for glass containers suitable for pharmaceutical use. They can be one of Type I, II, or III. Type I is made of neutral borosilicate glass as shown in Figure 1, Type II is made of soda-lime glass and Type III is made of untreated soda-lime glass. Every year over 35 to 45 billion such containers are produced [1]. Various factors like usability, storage, administration, sterility to prevent contamination, compatibility with the drug formulation to prevent interactions or leaching, and protection of the drug from environmental factors like light, moisture, and oxygen play important roles in selecting the type of container for pharmaceutical use. Various types of plastic bottles such as high-density polyethylene (HDPE) bottles, polypropylene (PP) bottles, and polyethylene terephthalate (PET) bottles are also in use as drug containers.

Figure 1. Pharmaceutical vial

Defect detection in pharmaceutical vials is critical for maintaining product integrity. Defects like cracks, black spots, wrinkles, bubbles, particles, delamination, or impurities can compromise the integrity of the product leading to potential risks for patients [1]. Breakages are very common during the production phase [2]. Delamination of glass will directly impact patient health and has resulted in the recalling of the drug product [3]. Delamination is due to the detachment of glass flakes within the vial and it results in contamination of drug fluid potentially affecting its safety and efficacy and needs to be addressed seriously. Traditional methods are time-consuming, often fall short in efficiency in identifying subtle defects, and prone to human error necessitating automated solutions for efficient and accurate defect detection. Figure 2 shows various types of cosmetic defects on the vial surface.



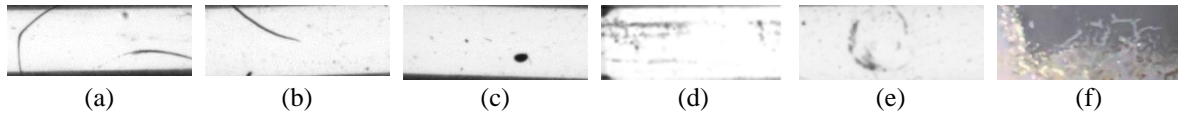|        |        |        |        |        |        |
| (a)    | (b)    | (c)    | (d)    | (e)    | (f)    |

Figure 2. Various defects on the vial (a) broken, (b) crack, (c) black spot, (d) scratches, (e) bubble, and (f) delamination

Integration of various defect detection strategies using machine vision is made to make machines more intelligent in the Industry 4.0 and onwards era [4]. This research proposes a methodology combining fast non-local means (FNLM) filtering with advanced image processing techniques to improve the accuracy and efficacy of defect detection in vials. In vial inspection, where images might have varying illumination or noise levels, FNLM's robustness ensures consistent defect detection across different conditions [5]. Phase stretch transform (PST) acts as an initial stage to capture potential anomalies in the vial images by extracting useful features related to textural variations and structural irregularities in the image. PST is based on the principles of differential interference contrast microscopy. It operates in the frequency domain and exploits the phase information contained within an image to enhance subtle features that might be otherwise challenging to detect [6]. PST extracts phase-related features by analyzing the phase congruency across different orientations and scales within the image. After PST feature extraction, subsequent processing steps like filtering, thresholding, and morphological operations are often applied to refine and localize the defects. Filtering aids in further refinement so that defects that are subtle get noticed by the system. Segmentation aids in identifying boundaries thus simplifying image representation [7]. Otsu thresholding, a widely used method for image segmentation, helps in distinguishing foreground from background [8]. Morphological operations like dilation aid in improving the continuity of detected regions, enhancing defect identification accuracy.

Previous studies have demonstrated the effectiveness of various image processing techniques in defect detection. The use of support vector machine (SVM), pulse-coupled neural network (PCNN), convolutional neural networks (CNN), and advanced non-destructive testing (NDT) are effective in the detection of defects on glass surfaces [9]. Smart manufacturing has led to better quality control in industries today through artificial vision, machine learning, and statistical process control [10].

CNNs are quite common among various defect detection techniques [11]–[13]. Defective caps on the bottles were found using a lightweight CNN model by Abhijit et al. [14] in high-speed production lines. Adam optimizer is introduced in the system to improve the parameters like weights and kernel values along with a cross-entropy loss module to increase the probability of detection. The model achieves better accuracy in identifying flawed bottle caps than existing methods. Despite challenges like side image capture and bottle classification issues, deep learning methods effectively address these issues, resulting in a 98% accuracy rate. A limitation of the study is its focus solely on bottle cap identification, as future research could expand the model's scope to detect liquid fill-levels, foreign particles, and label alignment deficiencies.

CNNs are popularly used in the detection of animals, pets, and other natural objects. DefectNet is a standard approach used for flaw detection [15]. MobileNet-v2-dense model was proposed by Lin *et al.* [16] for better detection of faults in woven fabrics. In this case, a standard function asymmetric loss function was introduced in the network to obtain better results. However, the study acknowledges limitations such as dataset diversity, generalization to other domains, and potential overfitting. Kazmi *et al.* [17] used simple techniques like hard thresholding for image binarization and identified defects on the plastic bottle at an accuracy rate of 95% without requiring high computation power or extensive training data, making it highly feasible for fast inspection. The systems inspected flaws on the cap, dent on the body, and the label. However, a notable weakness lies in the limited capability of the system compared to artificial intelligence (AI) based algorithms. Malesa and Rajkiewicz [18] developed an exclusive system for pet bottle inspection using a deep neural network. The methodology involved the calibration of a system using a checkerboard pattern for image acquisition followed by an inspection framework using the CustomKSM approach. This approach significantly reduces prediction and training times without sacrificing accuracy but has a limited scope of application to specific industries and production lines. Zhou *et al.* [19] BTMfast technique to find defects in the body of the glass bottle. The method used Otsu thresholding to segment the template of each image, then binary template matching (BTM) is applied on a filtered image to obtain the bottle mouth boundary at the top portion and the defect is identified. The strengths of the framework include its ability to reduce computational complexity through down sampling and obtain accurate localization results with a low localization error of about 1.5 and a faster processing time of approximately 4.3 ms. However, its drawback is the limited evaluation datasets, which may not fully represent real-world scenarios.

A segmentation approach based on CNN was proposed by Lu *et al.* [20] for flaw detection on the surfaces. A network MRD-Net which is obtained using the networks multiscale feature enhancement fusion (MFEF) and reverse attention (RA) was used. The MobileNetV2 model was pre-trained to extract feature maps on multiscale and obtained good accuracy on small size samples. Gong *et al* [21] used deformable template matching for defect localization on the labels of the bottle. Even minute defects were detected by applying adaptive thresholding on the labels with Chinese letters. However, the scope is limited only to labels of the bottle. Lv *et al.* [22] improvised YOLOv3 and used four scales to detect even minute objects. A spatial pyramid structure was introduced to find flaws in the glass with an accuracy value of 97.66%. Ma *et al.* [23] used the ensemble learning (EL) approach for flaw detection of medicine bottles. Acquired images were pretreated to reduce the variation effect caused due to the change in lighting condition. Multiple features were extracted for the effective detection of flaws. The system features a tunnel structure that seamlessly integrates into existing processes and devices, ensuring automated inspection without disruption. Leveraging a high-precision vision detection method, the system employs a local background difference approach and image gray-level equalization preprocessing to mitigate illumination effects. A virtual simulation inspection was proposed in [24] to illustrate the flaw detection in beer bottles. However, the study was limited to virtually demonstrating how flaws can be found in beer bottles, and therefore its practicality is very limited in scope. Similarly, a modeling and animation application was proposed to utilize the game engine UE4. Xu and Huang [25] proposed SC-CAENet, for glass defect detection, addressing challenges in manual annotation acquisition. By employing a convolutional auto-encoder followed by image difference computation, the method effectively detects defect regions. The introduction of skip connections and weighted structural similarity loss enhances detection precision. The outcomes with SC-CAENet show an accuracy of 0.9475, along with low escape and overkill rates, detecting defects in just 32 ms per image. However, its potential weaknesses may include limitations in handling complex defect patterns and variability in glass types. He *et al.* [26] introduced an inspection system high-angle and multi-view (HAMV) to detect bottle cap defects. The method used the background reconstruction of line structure element (BRLSE) technique which focused on the use of line structure elements for background texture reconstruction. Non-skid bar interference was eliminated to a great extent to detect flaws effectively. The system inspected 400 pieces of caps in a minute at an accuracy of more than 95%.

Sari and Ulas [27] proposed a deep learning model based on YOLOv3 for defect detection of glass jar surfaces. Achieving a performance of 94.65% for raw data, the study explores color space conversion (CSC) techniques, specifically hue, saturation, value (HSV) and CIE-Lab Luv, for image preprocessing. While the HSV method shows a decrease in performance, the CIE-Lab Luv method, particularly with adaptive histogram equalization, exhibits significant improvements, with maximum recall, precision, and F1-score surpassing 97%. Furthermore, comparative analysis with Faster R-CNN demonstrates YOLOv3's superior performance, especially when combined with adaptive histogram equalization in the CIE-Lab Luv method. Xie *et al.* [28] proposed FE-YOLO model for real-time applications. The YOLO model was improvised by introducing a network based on a feature pyramid and a prediction box regression model. k-means++ was used later to enhance the convergence and obtain better detection accuracies compared to existing YOLO-based models. Mao *et al.* [29] proposed an advanced network Dy-YOLOv5s based on deep learning for flaws inspection of smartphone glass. The study proposed a model called dynamic head for the

detection of flaws dynamically. Hu *et al.* [30] proposed low-light enhancement and multi-scale feature extraction (LE–MSFE–DDNet) to detect flaws in the images taken in dim lighting conditions. They introduced a block to overcome illumination variability along with the use of the SE-FP model. The multi-scale feature extraction technique applied after this stage resulted in effective flaw detection with an average accuracy of 94.3%. An inspection system developed by Wang *et al.* [11] for detecting scale defects on medical syringes. By proposing a two-stage framework comprising a scale extraction network (SeNet) and a scale defect discriminator (SDD), the study offers an innovative approach to defect localization. SeNet effectively extracts the main structure of scales, while SDD detects and labels scale defects. The strengths of the method lie in its ability to achieve high detection performance with a small number of negative samples. However, the limitation may include the need for further validation across diverse syringe manufacturing environments and defect variations to ensure robust performance in real-world settings. Tang *et al.* [31] used extraction of adaptive boundary and essential features, cropped the images to get uniform configurations, and then produced masked images which are fed into the detection system to detect defects on the aluminum profile using mean structural similarity index measure (MSSIM) comparison. The accuracy of the system reached 97.7%. Various approaches were proposed to detect flaws on the surface. The features like color, texture, and shape are considered for the study [32]. Many approaches were proposed for defect detection on steel surfaces [33]. Deshpande *et al.* [34] used a Siamese CNN system to identify flaws on the steel surface and obtained a testing accuracy of 92.55%. Cao *et al.* [35] used the YOLOv7 model for flaw detection on the chip package. Anchor frames were clustered using K-means++, CBAM was merged with RFB structure, and as a result, CP-Cluster was introduced which led to an increase in the accuracy of flaw detection. Deep learning models are in use for the detection of surface defects [36], [37]. A deep learning model based on ResNet50 was proposed by Yang *et al.* [38]. Here, feature extraction was done using MCF block for performance enhancement of the technique.

A segmentation and deep learning based approach was adopted by Tabernik *et al.* [39], [40] for crack detection on the surface. There are models based on continuous incremental learning for enhancing the detection of any new type of defects. These AI enabled incremental systems facilitate learning either by implementing class or task models. This model proposes the concept of lifelong learning having various steps such as data acquisition, data analysis, expert interviews, data pre-processing, data labeling, training the model, and model deployment. The system will be updated continuously with new categories of data until no new data is available [41].

From the studies addressing bottle defects to glass product quality control and medical syringe scale detection, from adaptive boundary extraction for aluminum profile defect detection to Siamese CNN systems for flaw identification on steel surfaces, each approach brings unique strengths and innovations to the field. Furthermore, the integration of deep learning models like YOLOv7 and ResNet50, along with continuous incremental learning approaches, demonstrates the evolving landscape of defect detection methodologies. Despite their strengths in accuracy and efficiency, these methods face challenges related to data requirements, computational complexity, and real-world applicability. Moving forward, the combination of innovative technologies with traditional machine vision approaches holds promise for enhancing defect detection systems across industries, providing further validation and refinement to ensure robust performance in diverse manufacturing environments.

The objective of the proposed method is to detect defects in pharmaceutical vials by addressing cracks, bubbles, black spots, and wrinkles. This study achieves this by integrating hybrid image processing techniques with PST. The structure of the paper is as follows: section 2 provides the methodology proposed for defect identification. Section 3 details the experiments conducted and the resulting outputs. Finally, section 4 presents the conclusions drawn from the study.

## 2. METHOD

The proposed system involves a multi-stage process utilizing hybrid image processing techniques for defect detection in pharmaceutical vials, as illustrated in Figure 3. This multi-stage process ensures a comprehensive analysis by integrating various advanced image processing methods, enhancing the accuracy and reliability of defect detection. By leveraging these techniques, the system effectively identifies and categorizes defects, improving quality control measures in pharmaceutical vial production.

The process starts with the image acquisition phase where good-resolution images of pharmaceutical vials are captured using a specialized industrial camera. The acquired images undergo preprocessing to enhance contrast, remove noise, and prepare them for subsequent analysis. In the preprocessing stage, FNLM filtering is applied to the acquired image to reduce noise and enhance image quality, preserving structural details. Then Gaussian low-pass filter is applied to further smooth the image, suppressing high-frequency noise. In vial images, where defects might be subtle and intertwined with the structure, preserving these

details is crucial for accurate defect detection. The phase features are extracted using the PST algorithm and it is then segmented using Otsu Thresholding. Otsu thresholding, a widely used segmentation method, aids in accurately separating defects from the background. Further refinement of defect-related features is carried out through Gaussian filtering for enhanced clarity. Morphological dilation is then applied to enhance defect regions, aiding in precise localization and boundary refinement. Then the potential defect areas are pinpointed by identifying regions of interest (ROI). The combination of these steps results in the localization of defects within the specified ROI. The contours represent the boundaries of the defects, and bounding rectangles are drawn around them for visualization and analysis. The decision whether to accept the vial or reject is made based on this step for better quality control assessment.
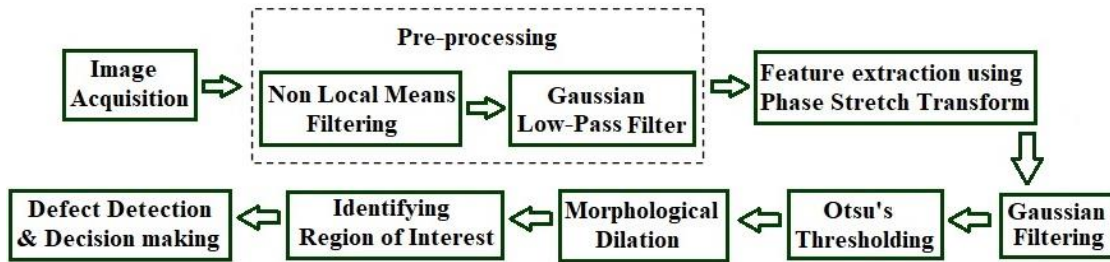


Figure 3. The flow of operations for defect inspection in pharmaceutical vials

## 2.1. Fast non-local means filtering

Fast non-local means (FNLM) filtering is a denoising technique commonly used in image processing. FNLM is adaptive and considers similarities among different image regions preserving structural information. In vial images, where defects might manifest as anomalies among otherwise uniform areas, adaptive filtering helps in distinguishing potential defects from the background. It effectively reduces noise without excessively smoothing edges or boundaries [42]. This is beneficial in vial images where defects might be located near edges or boundaries, ensuring that these defect-related details are retained. The FNLM is defined as in (1):

$$NLM[g](p) = \sum_{q=I} w(p,q)g(q) \tag{1}$$

where the acquired unfiltered image is denoted by $g$ whose coordinate values are represented by $p$ and $q$. The distance weight is represented by $w(p,q)$ whose pixel similarity is given by $p$ and $q$ with the condition $0 \leq w(p,q) \leq 1$ satisfied. The distance weight $w(p,q)$ is defined as in (2):

$$w(p,q) = \frac{1}{Z(p)} e^{-\frac{\|u(j_p)-u(j_q)\|_{2,a}^2}{d^2}} \tag{2}$$

In (2), the weighted Euclidean distance is represented by the term $\|u(j_p) - u(j_q)\|_{2,a}^2$. In this, the standard deviation is given by $a$ and filtering effectiveness is represented by the smoothing variable $d$. The term $Z(p)$ is a constant value representing a normalized factor. It is given as in (3):

$$Z(p) = \sum_{q} e^{-\frac{\|u(j_p)-u(j_q)\|_{2,a}^2}{d^2}} \tag{3}$$

## 2.2. Phase stretch transform

In the defect detection process, phase stretch transform (PST) serves as a powerful initial step in feature extraction. The PST is a computational imaging technique that can effectively capture and analyze textures, shapes, and structural features within an image. PST is used for extracting features based on phase information that helps to identify potential defects in the vial images focusing on textural variations and structural anomalies. PST emphasizes identifying irregularities that may signify cracks, impurities, or bubbles on the surface of the vials. It highlights variations in the image's phase to identify potential defects.

A 2D phase kernel function is used for finding edge-related spatial information in PST. This information is represented in the frequency domain. Suppose a vial image is in a higher frequency domain, then PST applies a high phase value thereby detecting edges based on frequency-dependent attributes. This

operation is represented as in (4), where $p$ and $q$ are 2D spatial values of the input image denoted by $G[p,q]$, whose phase profile output is defined by $F(p,q)$.

$$F(p,q) = \angle \langle IFFT2\{K[i,j] \cdot L[i,j] \cdot FFT2\{G[p,q]\}\}\rangle \qquad (4)$$

where $\angle$ denotes the angle operator, 2D fast Fourier transform (FFT) is denoted by $FFT2$ and 2D inverse fast Fourier transform is denoted by $IFFT2$, $i$ and $j$ are 2D frequency parameters. $L[i,j]$ denotes the localization kernel's frequency response and the warped phase kernel is denoted by $K[i,j]$ which is a nonlinear frequency-dependent phase defined as in (5):

$$K[i,j] = e^{c \cdot \varphi[i,j]} \qquad (5)$$

The phase kernel derivative profile is denoted by $PD[i,j]$ is considered to be a linear function concerning parameters $i$ and $j$. Such profile is obtained by using an inverse tangent function producing the PST kernel phase as given in (6):

$$\varphi[i,j] = \varphi_{polar}[r,\theta] = \varphi_{polar}[r]$$
$$= S \cdot \frac{W \cdot r \cdot tan^{-1}(W \cdot r) - \left(\frac{1}{2}\right) \cdot \ln(1 + (W \cdot r)^2)}{W \cdot r_{max} \cdot tan^{-1}(W \cdot r_{max}) - \left(\frac{1}{2}\right) \cdot \ln(1 + (W \cdot r_{max})^2)} \qquad (6)$$

where $r = \sqrt{i^2 + j^2}$, $\theta = tan^{-1}(j/i)$ and $r_{max}$ denotes the max frequency $r$. The phase profile parameters warp and strength are represented by $W$ and $S$ respectively. They are used to build phase localization kernels and help extract the edge information using the threshold values generated.

The PST-extracted features related to phase information serve as a basis for subsequent processing steps in the defect detection pipeline. These features are often refined and analyzed further using additional image processing techniques to precisely localize and classify the defects within the vial images.

### 2.2.1. Algorithm for feature extraction using PST

The algorithm involves transforming the image, constructing a PST kernel, extracting phase features, and performing morphological operations to detect potential defects based on phase variations.

1) Initialization:
   Set the parameter $L = 0.5$. Generate a mesh grid representing the image coordinates within the range of $-L$ to $L$ for both the x and y axes.
2) Conversion to polar coordinates:
   Convert the Cartesian coordinates $i, j$ to polar coordinates (THETA, RHO).
3) Localization kernel application to reduce noise:
   Apply a localization kernel to the original image in the frequency domain to reduce noise. This involves: i) Fourier transforming the original image I; ii) Constructing and applying an exponential filter (expo) based on frequency distance (RHO) to the Fourier-transformed image to reduce noise; iii) Inverse Fourier transforming the filtered image to obtain filtered image represented as *Image_orig_filtered*.
4) PST kernel construction and application:
   Construct a PST kernel (*PST_Kernel*) based on the frequency distance (RHO) and user-defined parameters (*Warp_strength* and *Phase_strength*). Apply the constructed PST kernel to the filtered image (*Image_orig_filtered*) in the frequency domain to obtain *Image_orig_filtered_PST*.
5) Feature extraction:
   Calculate the phase of the transformed image (*PHI_features*) obtained from the PST.
   If *Morph_flag* is 0, the output is the phase features (*out=PHI_features*).
   If *Morph_flag* is not 0, further processing steps for defect detection are executed:
   − Threshold the phase image (*PHI_features*) to identify sharp transitions using user-defined thresholds (*Threshold_max* and *Threshold_min*) and remove noise from dark areas.
   − Perform binary morphological operations (thin, perimeter extraction, erode) to enhance defect features in the transformed image.

The PST technique can be effective for detecting defects in vial images by reducing noise, preserving edges, enhancing contrast, and providing a more suitable input for subsequent image processing steps.

### 2.3. Gaussian filtering

Gaussian filtering is applied after PST to enhance the extracted features, further highlighting relevant structures or defects. This stage improves the visibility of defects by adjusting the local contrast,

making subtle anomalies more discernible. Consequently, the image is better prepared for further refinement in the defect detection process, ensuring more accurate and reliable results.

## 2.4. Otsu thresholding

Otsu's thresholding method is employed to determine optimal thresholds resulting in precise segmentation of defects from the background for better identification of subtle defect areas extracted using PST. The method works on the image and segregates it into two classes of pixels with distinct intensity levels, and it generates an optimum threshold value that minimizes the intraclass variance and maximizes the interclass variance. To do it, the method first computes the histogram of the input image. The histogram is then normalized to generate probability mass functions for the foreground (object) and background (non-object) classes. The interclass variance for each possible threshold $t$ is given by (7) as:

$$\sigma_b^2(t) = P_0(t) \cdot (\mu_0(t) - \mu)^2 + P_1(t) \cdot (\mu_1(t) - \mu)^2 \tag{7}$$

where $P_0(t)$, $\mu_0(t)$ and $P_1(t)$, $\mu_1(t)$ represents cumulative probabilities and mean intensities for the two classes of images. The global mean intensity of the entire image is given by (8) as:

$$\mu = \sum_{i=0}^{L-1} i \cdot P(i) \tag{8}$$

where $L$ represents the number of intensity levels. The optimal threshold value $t$ is generated based on the maximum value generated for $\sigma_b^2(t)$ is given by (9) as:

$$t_{optimal} = max_t \, \sigma_b^2(t) \tag{9}$$

where $t_{optimal}$ represents the threshold value that can effectively segment the foreground and background in a way that maximizes the interclass variance. This step is followed by the application of Gaussian filtering to refine defect features further.

## 2.5. Morphological dilation and ROI identification

To increase defect detection accuracy, it is important to enhance the clarity of defect regions and facilitate its accurate localization dilate morphological operation is used. Morphological dilation is typically performed using a structuring element (kernel). The basic idea is to slide the kernel over the image, and at each position, if the kernel overlaps with foreground (non-zero) pixels, the center of the kernel is set to the foreground in the resulting image.

For a binary image $A$ and a structuring element $B$, the dilation operation $A \oplus B$ is defined in (10).

$$A \oplus B(i,j) = \bigcup_{(p,q) \in B} A(i+p, j+q) \tag{10}$$

where the pixel coordinates are represented by $(i,j)$ and the coordinates of the structuring element is represented by $(p,q)$. Morphological dilation aids in the identification of ROIs based on the processed image, focusing on areas showing potential defects.

## 2.6. Defect detection and decision-making

Defect detection is done by narrowing down to a specific area of interest (ROI) and finding the exact locations of defects within that region. This involves determining contours within the ROI and drawing rectangles around the identified defects. The visualization includes a transparent rectangle for the ROI and white rectangles around the defects. This localized information is useful for analysis, visualization, and further decision-making in quality control or inspection applications.

## 3. RESULTS AND DISCUSSION

Dataset Description: Due to the specialized nature of the research domain and the lack of publicly available datasets tailored for vial defect inspection, an in-house dataset was curated. Recognizing the limitations inherent in the dataset, including its size and diversity, measures were taken to mitigate bias through extensive augmentation (rotation and scaling) and validation procedures.

Figure 4 illustrates the setup designed for capturing vial images, comprising a Nebula LED backlight serving as the light source, an industrial camera, a conveyor, and a desktop computer. The Nebula LED backlight (Nebula-80R) was chosen for its customizable brightness levels, providing adaptability to varying lighting conditions. For precise image acquisition, a Tamron machine vision camera (5MP, VCXG-52MR)

paired with a 50 mm Baumer lens (M118FM50) was utilized. This camera-lens combination offers advanced features such as auto-focus and image stabilization, ensuring high-quality images crucial for accurate defect detection. Moreover, the setup's versatility enables seamless integration into existing machine vision systems, facilitating automation and enhancing production efficiency. The desktop computer, equipped with a 2.8 GHz, 5th generation core i5 processor, 8 GB of RAM, GPU (Nvidia RTX 3070) operating at a frequency of 1,500 MHz, and 1 TB of storage space, completes the configuration. The image samples are monochrome images having reasonably good resolution.

Figure 4 illustrates the setup designed for capturing vial images, comprising a Nebula LED backlight serving as the light source, an industrial camera, a conveyor, and a desktop computer. Figure 4(a) shows the camera positioned for vial image capture, while Figure 4(b) displays the vial placed with a backlight for image capture. These configurations are critical for achieving high-quality images necessary for accurate defect detection.
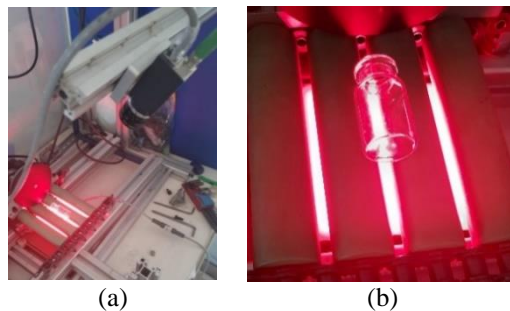


(a)                           (b)

Figure 4. System setup for vial image capture (a) camera positioned for vial image capture and (b) vial placed with backlight for image capture
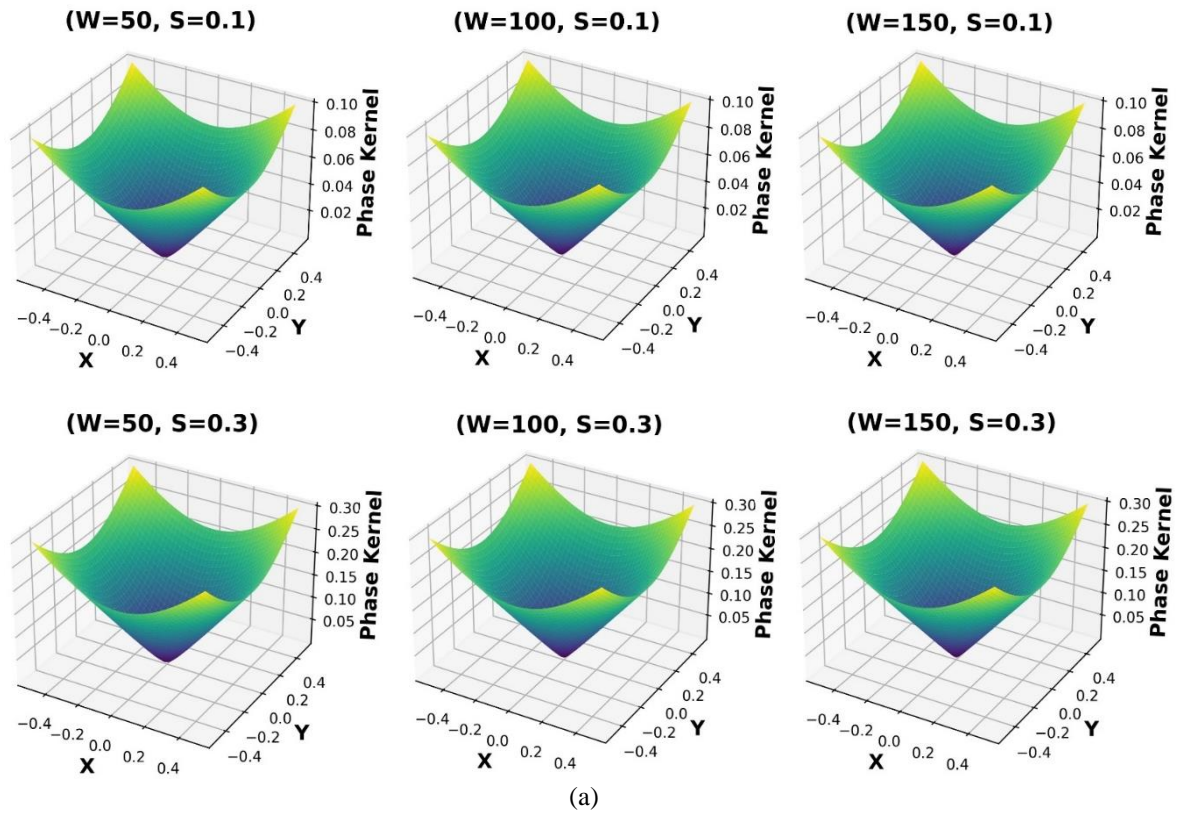
The implementation of the proposed technique is done using Python. Degree of smoothing (DoS) for NLMF was set to 25 for better results. The image is then preprocessed using a Gaussian low pass filter to further smoothen the image.

The step for phase feature extraction involves initializing parameter ($L$) that represents half of the spatial range used to create the mesh grid of coordinates ($i, j$) within a range (-0.5 to 0.5) based on the shape of the input image represented by $I$ and it controls the spatial domain of the generated phase kernels. These generated coordinates are converted to polar coordinates θ, $r$ (THETA, RHO) respectively. A localization kernel is created to reduce noise in the original image ($I$) by applying a frequency-domain operation. It calculates a filter that acts on the Fourier-transformed image. The PST kernel is then constructed using the calculated polar coordinates (RHO) and edge detection parameters warp strength ($W$) and phase strength ($S$). The values of $W$ and $S$ affect each frequency's phase along with the PST kernel structure and also its derivative profile. Figure 5 shows the 2D phase kernels and their corresponding derivative profiles for six different values of $W$ and $S$ variables. Figure 5(a) illustrates the 2D phase kernels, while Figure 5(b) depicts the 2D phase derivative profiles. The figure shows the effect of $W$ and $S$ variables on phase kernel structure. This kernel is applied to the filtered image to perform the PST transformation, yielding an image that is processed using PST. Then the phase angle of each pixel is extracted from the PST-transformed image. To do this, localization and PST transformation needs to be applied. This information characterizes the phase shift introduced by the PST and can highlight structural variations in the image related to potential defects.

Figure 6 shows various stages of the vial defect detection process for a sample image with a crack on its body. The phase image is generated using 2D IFFT by converting the frequency domain to the spatial domain. The figure includes the original image, nonlocal means filtering, feature extraction using PST, Gaussian filtering, Otsu's thresholding, morphological dilation, identifying ROI, ground truth image, and defects highlighted, as shown in Figures 6(a) to 6(i). These stages illustrate the transformation of the image through various processing steps to accurately detect and highlight defects.

The phase of the transformed image is thus calculated. Then thresholding is applied to identify sharp transitions in the phase image, marking potential defect areas. Pixels with phase values above the maximum threshold value or below the minimum threshold value are marked as potential defects. Additionally, very dark areas in the original image are considered as noise and are removed. Binary morphological operations (thin, perimeter extraction, and erosion) are performed to refine and enhance the potential defect areas, resulting in the PST phase output as shown in Figure 6(c).
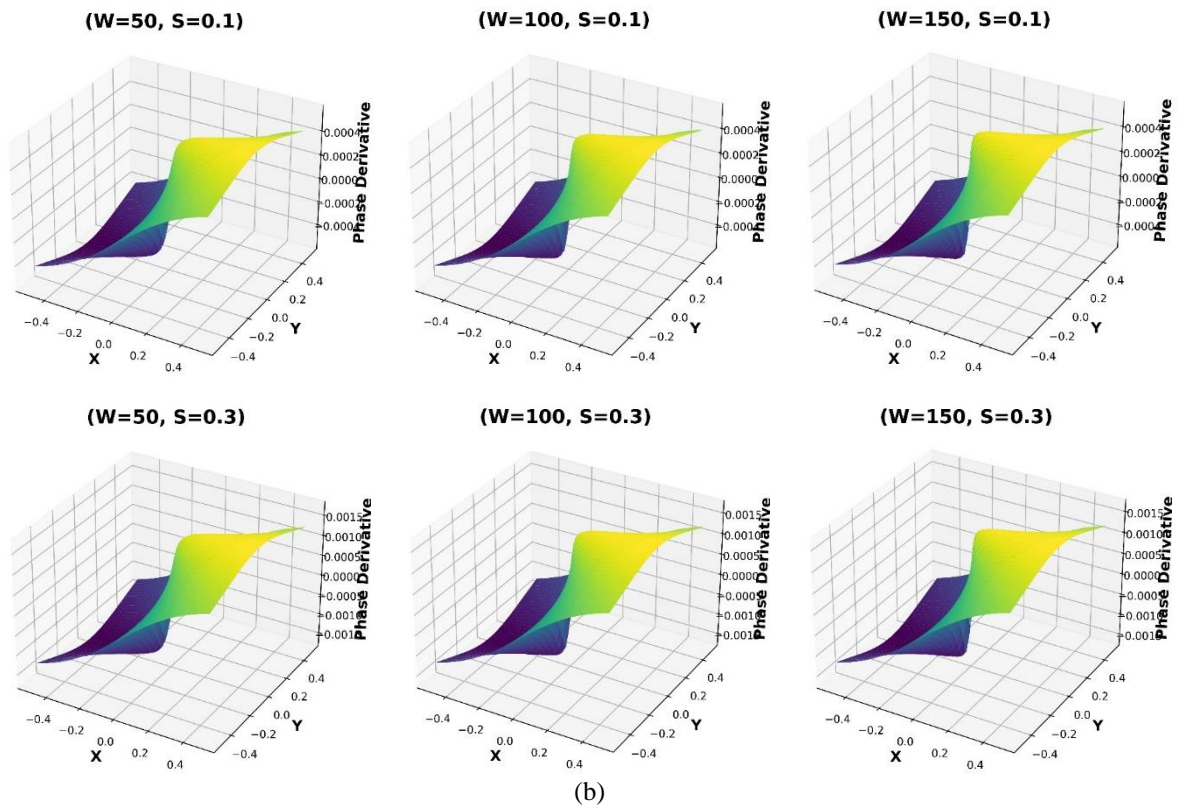
## 2D Phase Kernels

**(W=50, S=0.1)**                **(W=100, S=0.1)**                **(W=150, S=0.1)**

**(W=50, S=0.3)**                **(W=100, S=0.3)**                **(W=150, S=0.3)**

(a)

## 2D Phase Derivative Profiles

**(W=50, S=0.1)**                **(W=100, S=0.1)**                **(W=150, S=0.1)**

**(W=50, S=0.3)**                **(W=100, S=0.3)**                **(W=150, S=0.3)**

(b)

Figure 5. Various values of *W* and *S* are used for obtaining (a) 2D phase kernels and (b) 2D phase derivative profiles

The output obtained after application of PST is post processed and segmented using Otsu. For identification of subtle defects, it is delayed further. A binary mask (*roi_mask*) is then created with the same dimensions as the processed dilated gray image. A white rectangle is drawn on the mask, representing the region of interest (ROI) where defects are expected to be present as shown in Figure 6(g). The rectangle is specified by its top-left and bottom-right coordinates (500, 260) and (1530, 380), respectively. A visualization of the ground truth is created by overlaying the *roi_mask* on the original processed gray image (dilated). The *roi_mask* is applied to the processed gray image, resulting in an image containing only the defects within the ROI. For each contour representing a defect within the ROI, a white bounding rectangle is drawn around each defect to visually highlight the identified regions on the *output_image* as shown in Figure 6(i). These rectangles highlight the identified defects. Here defects are identified by finding contours within a masked region of the image. Each contour represents the boundary of a defect. Adjusting the alpha values allows for better visualization of the overlay and transparency.

Figure 7 shows the 3D PST kernel and 3D derivative profile generated for the sample vial image given in Figure 6. The total time taken by the system to detect the defect was 6.4 ms. The sensitivity is calculated by comparing the phase image with the ground truth image. Table 1 shows the sensitivity obtained for various values of *W* and *S* along with a graph for the sample vial image. From Table 1, it can be observed that for the given vial image with crack, the best sensitivity obtained is 0.986 when the value of *W* and *S* is set to 30 and 0.3 respectively. Therefore, the same values of *W* and *S* are used in the experiment. Figure 8 shows the sensitivity evaluation graph for various values of *W* and *S*.
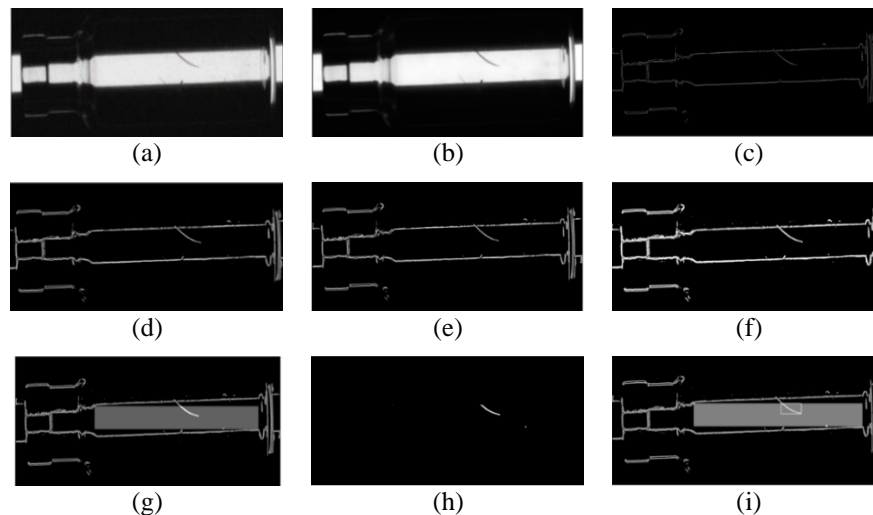


Figure 6. Sample output of the proposed technique (a) original image, (b) nonlocal means filtering,
(c) feature extraction using PST, (d) Gaussian filtering, (e) Otsu's thresholding, (f) morphological dilation,
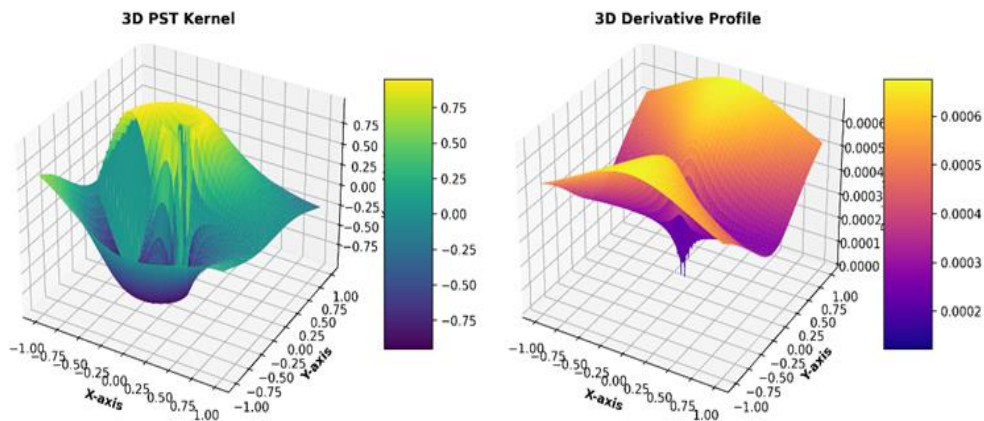(g) identifying ROI, (h) ground truth image, and (i) defects highlighted



Figure 7. 3D PST kernel and 3D derivative profile generated for the sample vial image

Table 1. Sensitivity evaluation for the sample vial image

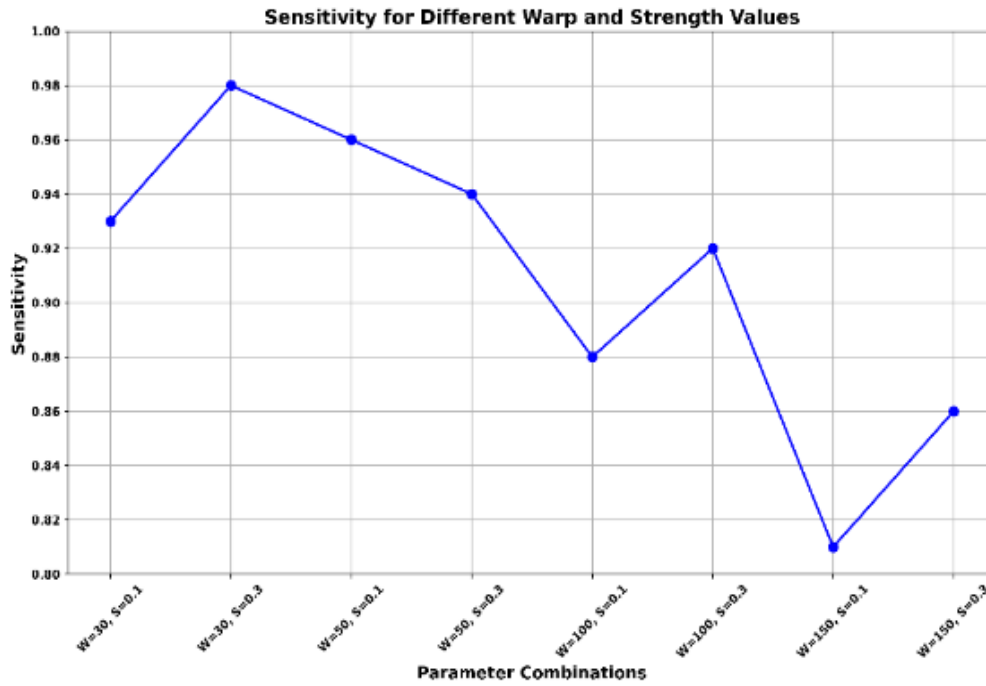| Warp (W) | Strength (S) | Sensitivity |
|---|---|---|
| 30 | 0.1 | 0.931 |
| 30 | 0.3 | 0.986 |
| 50 | 0.1 | 0.962 |
| 50 | 0.3 | 0.941 |
| 100 | 0.1 | 0.883 |
| 100 | 0.3 | 0.921 |
| 150 | 0.1 | 0.814 |
| 150 | 0.3 | 0.864 |



Figure 8. Sensitivity evaluation graph

## 3.1. Evaluation

Evaluation of the proposed system is carried out in terms of recall (sensitivity), accuracy, precision, specificity, and F1-score as given in Table 2. where true positive (TP), true negative (TN), false positive (FP), and false negative (FN) are the parameters used in their absolute meaning. Table 2 shows various evaluation metrics with their mathematical expressions.

Table 2. Proposed evaluation metrics with their mathematical expression

| Performance metric | Formula |
|---|---|
| Recall/Sensitivity | $\dfrac{TP}{TP + FN}$ |
| Accuracy | $\dfrac{TP + TN}{Total\ Sample}$ |
| Precision | $\dfrac{TP}{TP + FP}$ |
| Specificity | $\dfrac{TN}{TN + FP}$ |
| F1-score | $2 * \dfrac{Precision * Recall}{Precision + Recal}$ |
| AUC_ROC | $\int_{0}^{1} TPR(FPR^{-1}(k))dk$ |
| AUR_PR | $\int_{0}^{1} Precision(k) \cdot \Delta Recall(k)dk$ |

The proposed methodology was implemented and tested on the curated dataset comprising diverse vial images with various defects on the surface. About 550 vials including defective and non-defective are tested using the proposed method and their outcomes are given in the confusion matrix shown in Figure 9. The obtained value for precision is 98.85%, recall is 98.57%, accuracy is 98.36%, specificity is 98.00%, and F1-score is 98.71% for the values provided in the confusion matrix. These metrics demonstrate the high performance of the proposed defect detection system. The high precision and recall values indicate that the system is both accurate and reliable in identifying defects, while the high F1-score reflects a balanced trade-off between precision and recall.

The area under the receiver operating characteristic curve (AUC-ROC) quantifies the performance of a classifier by evaluating both its true positive rate (sensitivity) and false positive rate. The true positive rate indicates the proportion of correctly identified defective items, while the false positive rate indicates the proportion of non-defective items incorrectly classified as defective. On the other hand, the area under the precision-recall curve (AUC-PR) assesses the trade-off between precision and recall. Precision gauges the accuracy of identifying defects among all items classified as defective, while recall (or sensitivity) measures the proportion of actual defective items correctly identified. The values of AUC-ROC and AUC-PR obtained are 98.18% and 99.08% respectively and are depicted in Figure 10.
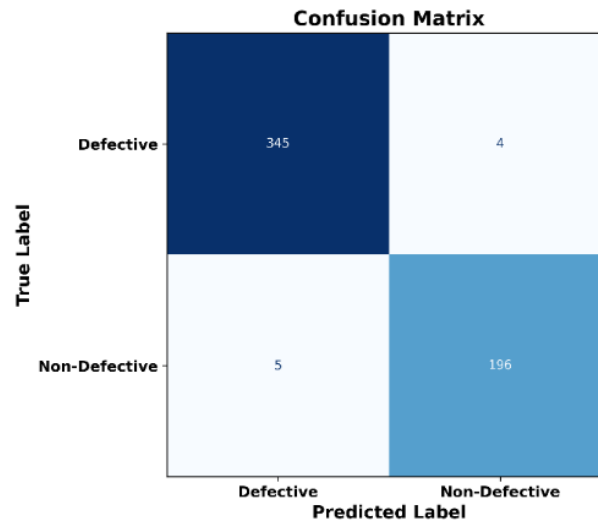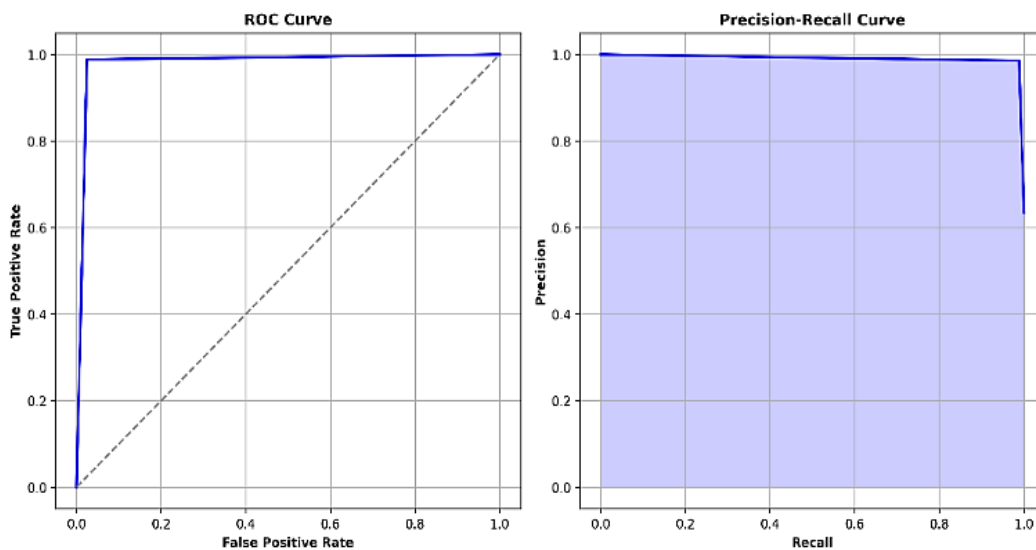


Figure 9. The confusion matrix



Figure 10. AUC-ROC and AUC-PR curve

The system achieved significant accuracy in detecting different types of defects, including cracks, black spots, bubbles, scratches, particles, and other impurities. Quantitative metrics, such as precision, recall, and F1-score validated the effectiveness of the approach in comparison to inspection methods cited in the literature. The comparison of the proposed method against various techniques or methodologies is given in Table 3. The respective comparative graph is shown in Figure 11. The comparison table illustrates that the methodology surpasses techniques outlined in the literature, achieving high performance metrics and demonstrating its robustness and industrial applicability.

Table 3. Summary of the performance of various methods

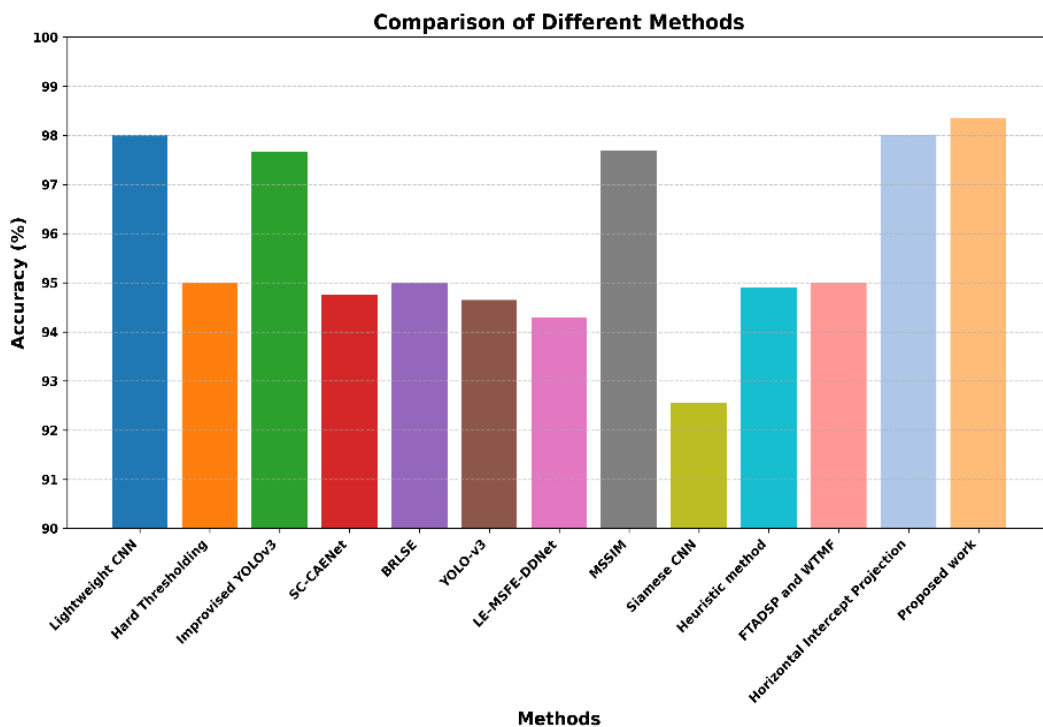| Sl. No. | Methodology | Accuracy |
| --- | --- | --- |
| 1 | Lightweight CNN [14] | 98.00% |
| 2 | Hard thresholding [17] | 95.00% |
| 3 | Improvised YOLOv3 [22] | 97.66% |
| 4 | SC-CAENet [25] | 94.75% |
| 5 | BRLSE [26] | 95.00% |
| 6 | YOLOv3 [27] | 94.65% |
| 7 | LE–MSFE–DDNet [30] | 94.3% |
| 8 | MSSIM [31] | 97.7% |
| 9 | Siamese CNN [34] | 92.55% |
| 10 | Heuristic method [43] | 94.9% |
| 11 | FTADSP and WTMF [44] | 95.00% |
| 12 | Horizontal intercept projection [45] | 98.00% |
| 13 | Proposed work | 98.36% |



Figure 11. Comparison of accuracy across different methods

## 4. CONCLUSION

This study has introduced an integrated methodology leveraging FNLM filtering and advanced image processing techniques for defect detection in pharmaceutical vials. The problem addressed is the detection of subtle defects such as cracks, bubbles, black spots, and wrinkles, which are critical to ensure the safety and efficacy of pharmaceutical products. The proposed solution combines FNLM filtering to improve image contrast and clarity, making subtle defects more discernible, with PST to enhance the capability to identify and characterize defects by leveraging phase information. PST's robustness to lighting variations and its effectiveness in highlighting phase-based anomalies make it particularly suitable for industrial settings.

The methodology involves creating a ROI, applying it to the PST-processed image, identifying contours within the ROI, and marking defects with rectangles. The results showcase the potential of the proposed approach to quality control processes in pharmaceutical manufacturing, ensuring the delivery of safe and reliable vials to consumers. The proposed approach has significantly enhanced defect identification accuracy compared to the techniques provided in the literature and can be adopted in industries for better quality control.

For future work, the system's capabilities, robustness, and usability can be further enhanced by integrating deep learning models such as convolutional neural networks. Implementing data augmentation techniques will increase the diversity of the training dataset, improving generalization across various lighting conditions, orientations, and defect types. Additionally, optimizing the system for real-time processing will facilitate rapid decision-making, further benefiting industrial applications.

## REFERENCES

[1]  D. Zuccato and E. Guadagnino, "Glass for pharmaceutical use," *Encyclopedia of Glass Science, Technology, History, and Culture*. Wiley, pp. 879–889, Feb. 2021, doi: 10.1002/9781118801017.ch7.7.

[2]  X. Jin, D. O'Grady, R. P. Affleck, S. Martini, and A. Saluja, "Freeze drying and vial breakage: misconceptions, root causes and mitigation strategies for the pharmaceutical industry," *Journal of Pharmaceutical Sciences*, vol. 113, no. 5, pp. 1306–1318, May 2024, doi: 10.1016/j.xphs.2023.12.010.

[3]  G. Kabirdas B and S. Sharda M, "Glass delamination in sterile formulations and drug recalls: a review," *International Journal of Pharmaceutical Sciences and Developmental Research*, pp. 006–115, Jan. 2022, doi: 10.17352/ijpsdr.000036.

[4]  Z. Ren, F. Fang, N. Yan, and Y. Wu, "State of the art in defect detection based on machine vision," *International Journal of Precision Engineering and Manufacturing-Green Technology*, vol. 9, no. 2, pp. 661–691, May 2021, doi: 10.1007/s40684-021-00343-6.

[5]  K. Chen, X. Lin, X. Hu, J. Wang, H. Zhong, and L. Jiang, "An enhanced adaptive non-local means algorithm for Rician noise reduction in magnetic resonance brain images," *BMC Medical Imaging*, vol. 20, no. 1, Jan. 2020, doi: 10.1186/s12880-019-0407-4.

[6]  M. H. Asghari and B. Jalali, "Edge detection in digital images using dispersive phase stretch transform," *International Journal of Biomedical Imaging*, vol. 2015, pp. 1–6, 2015, doi: 10.1155/2015/687819.

[7]  D. Honzátko, E. Türetken, S. A. Bigdeli, L. A. Dunbar, and P. Fua, "Defect segmentation for multi-illumination quality control systems," *Machine Vision and Applications*, vol. 32, no. 6, Sep. 2021, doi: 10.1007/s00138-021-01244-z.

[8]  A. L. Siridhara, K. V. Manikanta, D. Yadav, P. Varun, and J. Saragada, "Defect detection in fruits and vegetables using K means segmentation and Otsu's thresholding," *2023 International Conference on Networking and Communications (ICNWC), Chennai, India, 2023, pp. 1-5*, doi: 10.1109/icnwc57852.2023.10127559.

[9]  C. R. Vishwanatha, V. Asha, S. More, C. Divya, K. Keerthi, and S. P. Rohaan, "A survey on defect detection of vials," in *Lecture Notes in Networks and Systems*, Springer Nature Singapore, 2023, pp. 171–186.

[10]  M. Galindo-Salcedo, A. Pertúz-Moreno, S. Guzmán-Castillo, Y. Gómez-Charris, and A. R. Romero-Conrado, "Smart manufacturing applications for inspection and quality assurance processes," *Procedia Computer Science*, vol. 198, pp. 536–541, 2022, doi: 10.1016/j.procs.2021.12.282.

[11]  X. Wang, X. Xu, Y. Wang, P. Wu, F. Yan, and Z. Zeng, "A robust defect detection method for syringe scale without positive samples," *The Visual Computer*, vol. 39, no. 11, pp. 5451–5467, Sep. 2022, doi: 10.1007/s00371-022-02671-3.

[12]  S. A. Singh and K. A. Desai, "Automated surface defect detection framework using machine vision and convolutional neural networks," *Journal of Intelligent Manufacturing*, vol. 34, no. 4, pp. 1995–2011, Jan. 2022, doi: 10.1007/s10845-021-01878-w.

[13]  A. Khan, A. Sohail, U. Zahoora, and A. S. Qureshi, "A survey of the recent architectures of deep convolutional neural networks," *Artificial Intelligence Review*, vol. 53, no. 8, pp. 5455–5516, Apr. 2020, doi: 10.1007/s10462-020-09825-6.

[14]  M. Abhijit and S. Shanmuga Priya, "Detecting faulty bottle caps using CNN model," *2021 2nd International Conference on Smart Electronics and Communication (ICOSEC)*, Trichy, India, 2021, pp. 1446-1452, doi: 10.1109/icosec51865.2021.9591780.

[15]  F. Li, F. Li, and Q. Xi, "DefectNet: toward fast and effective defect detection," *IEEE Transactions on Instrumentation and Measurement*, vol. 70, pp. 1–9, 2021, doi: 10.1109/tim.2021.3067221.

[16]  Z. Lin, H. Ye, B. Zhan, and X. Huang, "An efficient network for surface defect detection," *Applied Sciences*, vol. 10, no. 17, p. 6085, Sep. 2020, doi: 10.3390/app10176085.

[17]  M. Kazmi, B. Hafeez, H. R. Khan, and S. A. Qazi, "Machine-vision-based plastic bottle inspection for quality assurance," in *IEEC 2022*, Jul. 2022, doi: 10.3390/engproc2022020009.

[18]  M. Malesa and P. Rajkiewicz, "Quality control of PET bottles caps with dedicated image calibration and deep neural networks," *Sensors*, vol. 21, no. 2, p. 501, Jan. 2021, doi: 10.3390/s21020501.

[19]  X. Zhou, Y. Wang, and Q. Zhu, "A fast and robust visual detection method with binary template matching for glass bottle body," Jul. 2019, doi: 10.23919/chicc.2019.8866571.

[20]  P. Lu, J. Jing, and Y. Huang, "MRD-Net: An effective CNN-based segmentation network for surface defect detection," *IEEE Transactions on Instrumentation and Measurement*, vol. 71, pp. 1–12, 2022, doi: 10.1109/tim.2022.3200361.

[21]  W. Gong, K. Zhang, C. Yang, M. Yi, and J. Wu, "Adaptive visual inspection method for transparent label defect detection of curved glass bottle," *2020 International Conference on Computer Vision, Image and Deep Learning (CVIDL)*, Chongqing, China, 2020, pp. 90-95, doi: 10.1109/cvidl51233.2020.00024.

[22]  H. Lv, S. Huang, W. Xie, Z. Chen, Z. Guo, and X. Zhang, "Multi-scale based defect detection for automotive glass," *Journal of Physics: Conference Series*, vol. 2303, no. 1, p. 12068, Jul. 2022, doi: 10.1088/1742-6596/2303/1/012068.

[23]  L. Ma, X. Wu, and Z. Li, "High-precision medicine bottles vision online inspection system and classification based on multifeatures and ensemble learning via independence test," *IEEE Transactions on Instrumentation and Measurement*, vol. 70, pp. 1–12, 2021, doi: 10.1109/tim.2021.3121465.

[24]  Y. Zhao, X. An, and N. Sun, "Virtual simulation experiment of the design and manufacture of a beer bottle-defect detection system," *Virtual Reality &amp; Intelligent Hardware*, vol. 2, no. 4, pp. 354–367, Aug. 2020, doi: 10.1016/j.vrih.2020.07.002.

[25]  H. Xu and Z. Huang, "Annotation-free defect detection for glasses based on convolutional auto-encoder with skip connections," *Materials Letters*, vol. 299, p. 130065, Sep. 2021, doi: 10.1016/j.matlet.2021.130065.

[26] C. He, C. Li, B. Chen, B. Yuan, and Y. Yin, "Research on defect detection of the outer side of bottle cap based on high angle and multi-view vision system," *IEEE Access*, vol. 11, pp. 65798–65809, 2023, doi: 10.1109/access.2023.3290616.

[27] F. Sari and A. B. Ulas, "Deep learning application in detecting glass defects with color space conversion and adaptive histogram equalization," *Traitement du Signal*, vol. 39, no. 2, pp. 731–736, Apr. 2022, doi: 10.18280/ts.390238.

[28] Y. Xie, W. Hu, S. Xie, and L. He, "Surface defect detection algorithm based on feature-enhanced YOLO," *Cognitive Computation*, vol. 15, no. 2, pp. 565–579, Oct. 2022, doi: 10.1007/s12559-022-10061-z.

[29] Y. Mao, J. Yuan, Y. Zhu, and Y. Jiang, "Surface defect detection of smartphone glass based on deep learning," *The International Journal of Advanced Manufacturing Technology*, vol. 127, no. 11–12, pp. 5817–5829, Jul. 2023, doi: 10.1007/s00170-023-11443-9.

[30] W. Hu, T. Wang, Y. Wang, Z. Chen, and G. Huang, "LE–MSFE–DDNet: a defect detection network based on low-light enhancement and multi-scale feature extraction," *The Visual Computer*, vol. 38, no. 11, pp. 3731–3745, Jun. 2021, doi: 10.1007/s00371-021-02210-6.

[31] S. Tang, Y. Zhang, Z. Jin, J. Lu, H. Li, and J. Yang, "A feature-oriented reconstruction method for surface-defect detection on aluminum profiles," *Applied Sciences*, vol. 14, no. 1, p. 386, Dec. 2023, doi: 10.3390/app14010386.

[32] Y. Chen, Y. Ding, F. Zhao, E. Zhang, Z. Wu, and L. Shao, "Surface defect detection methods for industrial products: a review," *Applied Sciences*, vol. 11, no. 16, p. 7657, Aug. 2021, doi: 10.3390/app11167657.

[33] Q. Luo, X. Fang, L. Liu, C. Yang, and Y. Sun, "Automated visual defect detection for flat steel surface: a survey," *IEEE Transactions on Instrumentation and Measurement*, vol. 69, no. 3, pp. 626–644, Mar. 2020, doi: 10.1109/tim.2019.2963555.

[34] A. M. Deshpande, A. A. Minai, and M. Kumar, "One-shot recognition of manufacturing defects in steel surfaces," *Procedia Manufacturing*, vol. 48, pp. 1064–1071, 2020, doi: 10.1016/j.promfg.2020.05.146.

[35] Y. Cao, Y. Ni, Y. Zhou, H. Li, Z. Huang, and E. Yao, "An auto chip package surface defect detection based on deep learning," *IEEE Transactions on Instrumentation and Measurement*, vol. 73, pp. 1–15, 2024, doi: 10.1109/tim.2023.3347799.

[36] Z. Jia, M. Wang, and S. Zhao, "A review of deep learning-based approaches for defect detection in smart manufacturing," *Journal of Optics*, vol. 53, no. 2, pp. 1345–1351, Aug. 2023, doi: 10.1007/s12596-023-01340-5.

[37] S. Qi, J. Yang, and Z. Zhong, "A review on industrial surface defect detection based on deep learning technology," in *2020 The 3rd International Conference on Machine Learning and Machine Intelligence*, Sep. 2020, doi: 10.1145/3426826.3426832.

[38] L. Yang, S. Bai, H. Huang, and S. Kong, "An automatic surface defect detection method with residual attention network," in *Lecture Notes in Computer Science*, Springer Nature Switzerland, 2022, pp. 194–205.

[39] D. Tabernik, S. Šela, J. Skvarč, and D. Skočaj, "Segmentation-based deep-learning approach for surface-defect detection," *Journal of Intelligent Manufacturing*, vol. 31, no. 3, pp. 759–776, May 2019, doi: 10.1007/s10845-019-01476-x.

[40] D. Tabernik, S. Šela, J. Skvarč, and D. Skočaj, "Deep-learning-based computer vision system for surface-defect detection," in *Computer Vision Systems*, Springer International Publishing, 2019, pp. 490–500.

[41] R. Mohandas, M. Southern, E. O'Connell, and M. Hayes, "A survey of incremental deep learning for defect detection in manufacturing," *Big Data and Cognitive Computing*, vol. 8, no. 1, p. 7, Jan. 2024, doi: 10.3390/bdcc8010007.

[42] S.-H. Kang and J.-Y. Kim, "Application of fast non-local means algorithm for noise reduction using separable color channels in light microscopy images," *International Journal of Environmental Research and Public Health*, vol. 18, no. 6, p. 2903, Mar. 2021, doi: 10.3390/ijerph18062903.

[43] M. Eshkevari, M. Jahangoshai Rezaee, M. Zarinbal, and H. Izadbakhsh, "Automatic dimensional defect detection for glass vials based on machine vision: A heuristic segmentation method," *Journal of Manufacturing Processes*, vol. 68, pp. 973–989, Aug. 2021, doi: 10.1016/j.jmapro.2021.06.018.

[44] X. Zhou *et al.*, "A surface defect detection framework for glass bottle bottom using visual attention model and wavelet transform," *IEEE Transactions on Industrial Informatics*, vol. 16, no. 4, pp. 2189–2201, Apr. 2020, doi: 10.1109/tii.2019.2935153.

[45] X. Liu, Q. Zhu, Y. Wang, X. Zhou, K. Li, and X. Liu, "Machine vision based defect detection system for oral liquid vial," in *2018 13th World Congress on Intelligent Control and Automation (WCICA)*, Jul. 2018, doi: 10.1109/wcica.2018.8630441.

## BIOGRAPHIES OF AUTHORS

**Vishwanatha C. R.** ⓘ 🔍 SC ◑ is an assistant professor at the Department of Master of Computer Applications, Nitte Meenakshi Institute of Technology, Bengaluru, India. Currently pursuing his Ph.D. at the research center in the Department of Computer Applications at New Horizon College of Engineering affiliated to Visvesvaraya Technological University, Belagavi, Karnataka, India. He specializes in machine vision algorithms. His research interests span computer vision, machine learning, and deep learning, and he has contributed to numerous research articles. His primary research directions include machine vision, machine learning, and automation. He can be contacted at email: vishwanathcr@gmail.com.

**Asha V.** ⓘ 🔍 SC ◑ holds a Ph.D. in computer science from the University of Mysore, Karnataka, India. She is a professor and head at the Department of Computer Applications, New Horizon College of Engineering, Bengaluru, India. She received her bachelor's and master's degrees in computer science from Mysore University. Her research interests include image processing, pattern recognition, machine learning, and information science. She has published research articles in various reputed Journals and presented her papers at various national and international conferences. She can be contacted at: asha.gurudath@gmail.com.